

Multi-Instrument Comparison of Top-of-Atmosphere Reflected Solar Radiation

NORMAN G. LOEB,^{*,**} BRUCE A. WIELICKI,⁺ WENYING SU,^{*} KONSTANTIN LOUKACHINE,[#] WENBO SUN,^{*} TAKMENG WONG,⁺ KORY J. PRIESTLEY,⁺ GRANT MATTHEWS,[@] WALTER F. MILLER,[#] AND R. DAVIES^{&,++}

^{*}Center for Atmospheric Sciences, Hampton University, Hampton, Virginia

⁺NASA Langley Research Center, and Hampton University, Hampton, Virginia

[#]Science Applications International Corporation, Hampton, Virginia

[@]Analytical Services and Materials, Hampton, Virginia

[&]Jet Propulsion Laboratory, California Institute of Technology, Pasadena, California

(Manuscript received 28 February 2006, in final form 23 June 2006)

ABSTRACT

Observations from the Clouds and the Earth's Radiant Energy System (CERES), Moderate Resolution Imaging Spectroradiometer (MODIS), Multiangle Imaging Spectroradiometer (MISR), and Sea-Viewing Wide-Field-of-View Sensor (SeaWiFS) between 2000 and 2005 are analyzed in order to determine if these data are meeting climate accuracy goals recently established by the climate community. The focus is primarily on top-of-atmosphere (TOA) reflected solar radiances and radiative fluxes. Direct comparisons of nadir radiances from CERES, MODIS, and MISR aboard the *Terra* satellite reveal that the measurements from these instruments exhibit a year-to-year relative stability of better than 1%, with no systematic change with time. By comparison, the climate requirement for the stability of visible radiometer measurements is 1% decade⁻¹. When tropical ocean monthly anomalies in shortwave (SW) TOA radiative fluxes from CERES on *Terra* are compared with anomalies in Photosynthetically Active Radiation (PAR) from SeaWiFS—an instrument whose radiance stability is better than 0.07% during its first six years in orbit—the two are strongly anticorrelated. After scaling the SeaWiFS anomalies by a constant factor given by the slope of the regression line fit between CERES and SeaWiFS anomalies, the standard deviation in the difference between monthly anomalies from the two records is only 0.2 W m⁻², and the difference in their trend lines is only 0.02 ± 0.3 W m⁻² decade⁻¹, approximately within the 0.3 W m⁻² decade⁻¹ stability requirement for climate accuracy. For both the Tropics and globe, CERES *Terra* SW TOA fluxes show no trend between March 2000 and June 2005. Significant differences are found between SW TOA flux trends from CERES *Terra* and CERES *Aqua* between August 2002 and March 2005. This discrepancy is due to uncertainties in the adjustment factors used to account for degradation of the CERES *Aqua* optics during hemispheric scan mode operations. Comparisons of SW TOA flux between CERES *Terra* and the International Satellite Cloud Climatology Project (ISCCP) radiative flux profile dataset (FD) RadFlux product show good agreement in monthly anomalies between January 2002 and December 2004, and poor agreement prior to this period. Commonly used statistical tools applied to the CERES *Terra* data reveal that in order to detect a statistically significant trend of magnitude 0.3 W m⁻² decade⁻¹ in global SW TOA flux, approximately 10 to 15 yr of data are needed. This assumes that CERES *Terra* instrument calibration remains highly stable, long-term climate variability remains constant, and the *Terra* spacecraft has enough fuel to last 15 yr.

1. Introduction

The exchange of radiant energy between the sun, earth, and space is fundamental to climate. The radia-

tive energy balance that exists between solar radiation absorbed by the earth and thermal infrared radiation emitted back to space regulates the earth's temperature and interacts directly with the components of the earth-atmosphere system such as clouds, the surface, and the atmosphere. The earth's outgoing fluxes have been observed to exhibit relatively large interannual variability during the past few decades: net radiation between 60°S and 60°N has a peak-to-peak range of ±0.7 W m⁻² and a standard deviation of 0.43 W m⁻² (Wielicki et al. 2002; Wong et al. 2006). This variability is similar in magnitude to the variability in ocean heat storage measurements (Wong et al. 2006), and the anticipated

^{**} Current affiliation: NASA Langley Research Center, Hampton, Virginia.

⁺⁺ Current affiliation: University of Auckland, Auckland, New Zealand.

Corresponding author address: Dr. Norman G. Loeb, NASA Langley Research Center, Mail Stop 420, Hampton, VA 23681-2199.
E-mail: n.g.loeb@larc.nasa.gov

change in anthropogenic radiative forcing over the next few decades ($\sim 0.6 \text{ W m}^{-2}$; Houghton et al. 2001). To achieve a more complete understanding of climate system variability, simultaneous independent observations of radiative fluxes and the earth-atmosphere components that influence the earth radiation budget are needed. Unfortunately, the majority of long-term satellite data records available today were derived from satellite instruments whose calibration accuracy and stability are too crude to detect anticipated trends in anthropogenic forcing. To move forward, therefore, we must take a hard look at our more modern instruments and determine whether or not they are meeting the accuracy requirements needed to address climate change.

To proceed, it is first necessary to define quantitatively, variable-by-variable, what the climate requirements are. Recently, Ohring et al. (2005) reported on an ongoing effort in which scientists from several satellite groups gathered for a workshop whose goal was to “develop requirements and recommend directions for future improvements in satellite instrument characterization, calibration, intercalibration, and associated activities to enable measurements of global climate change that are valid beyond a reasonable doubt.” The group produced a set of accuracy requirements for approximately 32 environmental variables derived from passive satellite instruments that make observations in spectral bands ranging from the ultraviolet to the microwave. Ohring et al. (2005) make a clear distinction between absolute accuracy and stability. Accuracy refers to the bias or systematic error of the data, while stability involves the extent to which the accuracy remains constant with time. Excellent absolute accuracy is vital for understanding climate processes and for model validation, whereas stability is needed for detecting long-term changes or trends in the data. As a result, stability requirements are generally more stringent than accuracy requirements. For example, Ohring et al. (2005) state that in order to meet climate requirements, imager visible radiances must provide visible cloud optical depth with an accuracy of 10% and a stability of $2\% \text{ decade}^{-1}$ (their Table 1), which lead to radiance requirements of 5% accuracy and $1\% \text{ decade}^{-1}$ stability (their Table 2). The equivalent Earth Radiation Budget instruments must produce shortwave (SW) top-of-atmosphere (TOA) fluxes with an accuracy of 1 W m^{-2} and a stability of $0.3 \text{ W m}^{-2} \text{ decade}^{-1}$. Since the climate requirement is based on SW cloud radiative forcing, we can simply convert the SW TOA flux stability requirement to radiance using $0.3/50 = 0.6\%$, where 50 W m^{-2} is the global average SW cloud radiative forcing. The Ohring et al. (2005) values are for an

uncertainty of $\pm 50\%$ in global cloud feedback. Reducing the feedback uncertainty to $\pm 25\%$ would require even tighter stability of $0.5\% \text{ decade}^{-1}$ for visible radiances, and $0.3\% \text{ decade}^{-1}$ for broadband SW radiances.

In this study, data from several state-of-the-art satellite instruments currently in orbit are analyzed and compared in order to determine whether or not data records emerging from these instruments appear to be meeting climate accuracy goals. The main emphasis here is on the stability of calibrated data records. The analysis is somewhat preliminary as it involves only up to 5 yr of data from each instrument. Comparisons performed include direct radiance comparisons for three instruments aboard the *Terra* spacecraft, and comparisons of deseasonalized anomalies in large-scale monthly mean quantities such as TOA reflected solar or SW flux. The main focus in this study is on SW radiation at the TOA. In the following, a detailed description of the observations from each instrument is provided, followed by comparisons of the relative stability and 5-yr monthly anomalies of data from the different instruments. Based on the initial 5-yr records, we employ commonly used statistical techniques to estimate the number of years of data needed to detect trends of comparable magnitude to the anticipated change in anthropogenic radiative forcing over the next few decades.

2. Observations

Table 1 provides a complete list of the datasets used in this study. The *Terra* satellite, launched in December 1999, is in a descending sun-synchronous near-polar orbit with an equator crossing time of 10:30 A.M. local time. Measurements from three of the five *Terra* instruments are considered. The Clouds and the Earth's Radiant Energy System (CERES) instrument (Wielicki et al. 1996) is a scanning thermistor bolometer that measures radiances in shortwave ($0.3\text{--}5 \mu\text{m}$), window ($8\text{--}12 \mu\text{m}$), and total ($0.3\text{--}200 \mu\text{m}$) channels at a spatial resolution of approximately $\sim 20 \text{ km}$ at nadir. CERES scans from limb to limb and provides global coverage each day. It can scan in three modes: cross-track, along-track, and rotating azimuth plane (RAP). Two CERES instruments, FM1 and FM2, are operating on *Terra*. The Moderate Resolution Imaging Spectroradiometer (MODIS) instrument (Salomonson et al. 1989; Barnes et al. 1998) measures narrowband radiances in 36 spectral bands from the visible to thermal infrared with a spatial resolution from 250 m to 1 km . It has a swath width of 2300 km and provides global coverage every 1–2 days. The Multiangle Imaging Spectroradiometer (MISR) instrument (Diner et al. 1998, 2002) provides

TABLE 1. List of datasets considered in this study.

Source	Parameter(s)	Product/version	Temporal coverage
CERES <i>Terra</i> (FM1)	SW unfiltered radiance, SW TOA flux	SSF Ed2B_rev1 (Loeb et al. 2005)	Mar 2000–Jun 2005
MODIS <i>Terra</i>	Nadir radiance in 0.64- and 0.86- μm bands, cloud fraction, aerosol optical depth	SSF Ed2B_rev1 (collection 4)	Mar 2000–Jun 2005
MISR <i>Terra</i>	Nadir radiance in 672- and 867-nm bands	SSFM Ed2B (collections 5 and 6)	Selected Sep days (2000–04)
CERES <i>Aqua</i> (FM4)	SW TOA flux	SSF Ed2A_rev1 (Loeb et al. 2005)	Aug 2002–Mar 2005
SeaWiFS SeaStar	Photosynthetically active radiation	Version 5.1	Mar 2000–Jun 2005
ISCCP	SW TOA flux	FD RadFlux (Zhang et al. 2004)	Mar 2000–Dec 2004

information on bidirectional reflectance anisotropy and geometric parallax using nine along-track angles from nadir to 70° in four visible/near-infrared spectral bands with a spatial resolution of 275 m – 1.1 km. MISR has a 400-km swath width and provides global coverage in 2–9 days, depending on latitude. Two identical copies of CERES (FM3 and FM4) and one MODIS instrument also fly onboard the *Aqua* spacecraft, launched in May 2002 in an ascending sun-synchronous near-polar orbit with an equatorial crossing time of 1:30 P.M. local time.

CERES, MODIS, and MISR all use onboard calibration sources to monitor instrument calibration stability. To monitor changes in gain over the mission lifetime, each CERES instrument has onboard calibration sources for every channel. Concentric groove blackbodies are used for the window and total channels, and a stable tungsten lamp is used for the SW channel. While the SW channel signal from the internal calibration lamps on CERES *Terra* has remained stable to the 0.2% level between 2000 and 2004 (Spence et al. 2004), comparison of independent observations from the two CERES *Terra* instruments indicates a decrease in reflected flux of 1.1% for FM1 and 1.6% for FM2 (Wielicki et al. 2005; Matthews et al. 2005). The effect was previously undetectable because the changes occurred in the blue-UV region, where tungsten lamp emission is very low. Direct comparisons of nadir radiance between CERES instruments in cross-track and hemispherical scan modes suggest that the decrease in instrument response to SW radiance occurs when CERES operates in a hemispherical scan mode. The decrease is believed to be associated with contaminant deposition on the optics while the CERES telescope is pointed in the direction of spacecraft motion, which only occurs when CERES is in a hemispherical scan mode. Consequently, when the CERES instrument operates in the cross-track scan mode (i.e., perpendicular to the direction of motion), there should be no degradation in the response to SW radiance. A table of adjustment coefficients (so called “rev1” adjustment factors; Matthews et al. 2005) has been derived for user

application to measurements made by CERES instruments on both *Terra* and *Aqua* satellites. Radiances and fluxes considered in this study have been adjusted using the rev1 factors derived in Matthews et al. (2005).

The MODIS design includes four onboard calibration modules: a solar diffuser, a solar diffuser stability monitor, a spectral radiometric calibration assembly, and a blackbody (Barnes et al. 1998). Two additional calibration techniques that MODIS uses are monthly views of the moon and deep space. A complete description of MODIS calibration performance during the first 4.5 yr in orbit is available in W. L. Barnes et al. (2004). The MISR instrument uses an onboard calibrator to provide updates to the instrument gain coefficients once every two months. The onboard calibrator consists of diffuse panels made of spectralon material and high quantum efficiency photodiodes, radiation-resistant photodiodes, and a goniometer (Bruegge et al. 2002).

The CERES and MODIS data considered are from the CERES Single Scanner Footprint TOA/Surface Fluxes and Clouds (SSF) product (Geier et al. 2003; Loeb et al. 2003). The SSF product merges CERES parameters including time, position, viewing geometry, radiances, and radiative fluxes with coincident information from MODIS, which is used to characterize the clear and cloudy portions of a CERES footprint. MODIS SSF parameters include radiances in five spectral bands for clear, cloudy, and total areas, cloud property retrievals (Minnis et al. 1998, 2003), and aerosol property retrievals from the MOD04 product (Remer et al. 2005), and a second aerosol retrieval algorithm applied to MODIS (Ignatov and Stowe 2002). Radiances from only two MODIS bands—MODIS bands 1 (0.645 or 0.65 μm) and 2 (0.858 or 0.86 μm)—are considered in this study. Pixel-level radiances and cloud retrievals from MODIS are averaged over CERES footprints after weighting by the CERES point spread function (PSF; Smith 1994; Loeb et al. 2003). Also included in the SSF product are meteorological parameters (e.g., surface wind speed, skin temperature, pre-

capitable water, etc.) from the Global Modeling and Assimilation Office's (GMAO's) Goddard Earth Observing System-Data Assimilation System (GEOS-DAS V4.0.3) product (Suarez 2005).

The MISR data used in this study are from the SSFM Edition2B data product (Loeb et al. 2006, hereafter LSMLD) for selected days in each September between 2000 and 2004. The SSFM dataset consists of MISR Level 1B2 radiances that have been averaged over CERES footprints with the same algorithm used to average MODIS pixel-level data in the SSF product. Each CERES footprint contains average radiances from each of the nine MISR directions in all four spectral bands. The SSFM data product is only produced for days when CERES scans in the along-track mode (approximately twice per month).

The Sea-Viewing Wide-Field-of-View Sensor (SeaWiFS; Hooker et al. 1992), launched in August 1997 onboard the *SeaStar* spacecraft, is an eight-band filter radiometer that measures radiances at 412, 443, 490, 510, 555, 670, 765, and 865 nm. SeaWiFS operates in a descending sun-synchronous polar orbit with a local noon equatorial crossing time. SeaWiFS uses routine lunar measurements (once per lunar month) to determine changes in its radiometric sensitivity (R. A. Barnes et al. 2004). Based on the lunar calibration methodology, Eplee et al. (2004) show that SeaWiFS TOA radiances are stable to better than 0.07% during the first 2500 days (6 yr and 10 months) since the first image was recorded. SeaWiFS daily (i.e., 24-h averaged) Photosynthetically Active Radiation (PAR) retrievals between March 2000 and June 2005 are considered here. PAR is defined as the solar flux reaching the ocean surface in the 400–700-nm spectral range. It is derived from SeaWiFS TOA radiance measurements in the PAR spectral range (Patt et al. 2003) and is provided for all-sky conditions over ocean only.

SW radiative fluxes from the International Satellite Cloud Climatology Project (ISCCP) radiative flux profile dataset (ISCCP-FD product; Zhang et al. 2004) for March 2000 through December 2004 are also considered. To create the ISCCP-FD product, global satellite measurements are used to specify 3-hourly cloud, atmosphere, and surface properties, which are input to a radiative transfer model to compute radiative fluxes at the TOA, surface, and several levels within the atmosphere. The ISCCP-FD product is an improved version of a previous ISCCP radiative flux product (ISCCP-FC; Zhang et al. 1995). A comprehensive description of the input data used to produce the ISCCP data product is provided in Zhang et al. (2004). The satellite imaging radiometers used by ISCCP are designed primarily for

weather applications for which accurate absolute calibrations were not emphasized (Rossow and Schiffer 1999; Brest et al. 1997). Therefore, there are no on-board calibration sources or lunar measurements available to monitor the stability of the reflected solar channels from these satellites. Rather, ISCCP must provide the absolute calibrations through vicarious methods (Brest et al. 1997).

3. CERES–MISR–MODIS radiance stability

Instrument calibration involves the use of both on-board calibration sources and vicarious calibration techniques to monitor and adjust the radiometric output of an instrument. If no calibration adjustments were made, most instruments would show significant levels of radiometric degradation (e.g., due to ultraviolet radiation exposure on the optics). The ability to compensate for instrument degradation through onboard sources and vicarious methods can only be done so accurately, however. Independent studies are thus needed to verify the stability of climate data records. This can involve examining time series of measurements from stable targets such as the moon, desert regions, deep convective clouds, etc., or intercomparisons amongst different calibrated instruments that observe the same region.

In the following, coincident measurements from CERES, MODIS, and MISR are used to quantify the relative stability of data records from these instruments during the first five years of operation. As there is no one instrument flying that serves as the calibration stability “standard” in space, it is not possible based on these results alone to claim that one data record is more stable than another. Nevertheless, a direct comparison does serve to identify any obvious discrepancies and provides preliminary data to assess whether or not data records emerging from the instruments appear to be meeting climate accuracy goals.

a. MODIS Terra and CERES Terra Radiance Comparison

CERES and MODIS *Terra* near-nadir radiances are compared in order to examine if radiances from these two instruments have been stable relative to one another during their first five years of operation. The comparison is restricted to CERES FM1 cross-track SW radiances and MODIS radiances in the 0.65- (band 1) and 0.86- μm (band 2) bands from the CERES SSF product. To minimize the influence of scene-dependent noise in the comparisons due to variations in the narrowband-to-broadband relationship between CERES

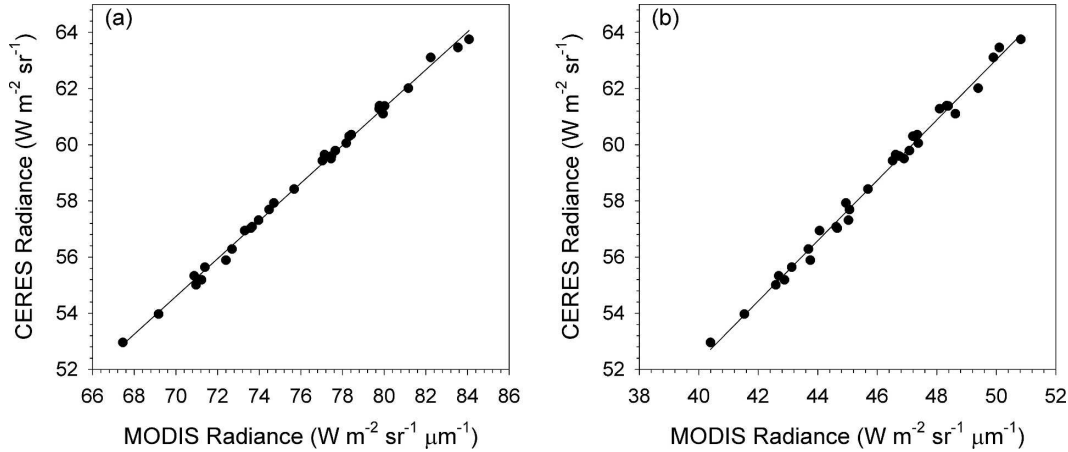


FIG. 1. Daily 30°N–30°S oceanic average CERES SW radiances against MODIS (a) 0.65- and (b) 0.86-mm radiance for May 2000. Lines correspond to regression fits to the data.

and MODIS with scene type (LSMLD), it is first necessary to average the CERES and MODIS measurements over relatively large spatial scales prior to determining their relative stability. Therefore, only CERES footprints over ocean between 30°S and 30°N with a viewing zenith angle smaller than 10° are considered. For each day of FM1 cross-track data between March 2000 and June 2005, average tropical ocean CERES SW and MODIS narrowband radiances are calculated from 1° latitude–longitude equal-area average values. A linear regression fit is then applied to the daily average CERES and MODIS radiances in each month (with CERES radiance as the dependent variable). Results for May 2000 are shown in Figs. 1a and 1b for the 0.65- and 0.86- μm MODIS bands, respectively. In the 0.65- μm band, the coefficient of determination (r^2) is 0.997 and the coefficient of variation (CV, defined as the standard deviation of the residuals divided by the mean) is 0.3%. Similarly, in the 0.86- μm band, r^2 is 0.993 and CV is 0.4%.

Next, the regression equations in each month are used to produce estimates of the overall mean predicted CERES SW radiance from all available daily tropical mean MODIS radiances. The predicted SW radiance based on regression coefficients in year (yr) and month (mn) is determined as follows:

$$\begin{aligned} \bar{I}_p^{\text{sw}}(\text{yr}, \text{mn}) &= \sum_{j=1}^{n_d} \frac{I_{p,j}^{\text{sw}}(\text{yr}, \text{mn})}{n_d} \\ &= \sum_{j=1}^{n_d} \frac{a_o(\text{yr}, \text{mn}) + a_1(\text{yr}, \text{mn})I_j}{n_d}, \end{aligned} \quad (1)$$

where a_o and a_1 are the intercept and slope of the regression, I_j is the daily tropical mean MODIS radiance

on day j , and n_d is the number of daily tropical mean MODIS radiances used (here $n_d = 1933$). The year-to-year relative stability of CERES and MODIS radiances is determined by comparing predicted mean CERES radiances from regression coefficients in each year with those in 2000 as follows:

$$\Delta(\text{yr}) = \frac{\frac{1}{n_m} \sum_{\text{mn}} \bar{\delta}(\text{yr}, \text{mn}) \pm t_{n_m-1} s_{\bar{\delta}}(\text{yr})}{\frac{1}{n_m} \sum_{\text{mn}} \bar{I}_p^{\text{sw}}(2000, \text{mn})}, \quad (2)$$

where

$$\bar{\delta}(\text{yr}, \text{mn}) = \bar{I}_p^{\text{sw}}(\text{yr}, \text{mn}) - \bar{I}_p^{\text{sw}}(2000, \text{mn}) \quad (3)$$

$$s_{\bar{\delta}}(\text{yr}) = \sqrt{\frac{\sum_{\text{mn}} [\bar{\delta}(\text{yr}, \text{mn}) - \bar{\bar{\delta}}(\text{yr})]^2}{n_m - 1}} \quad (4)$$

$$\bar{\bar{\delta}}(\text{yr}) = \sum_{\text{mn}} \frac{\bar{\delta}(\text{yr}, \text{mn})}{n_m}, \quad (5)$$

t_{n_m-1} is derived from the Student's t distribution for $n_m - 1$ degrees of freedom at the 95% significance level, and n_m is the number of months in which FM1 cross-track data are available in both yr and in 2000. If both CERES and MODIS radiances remained perfectly stable during the first five years of operation, or if the radiances of both instruments drifted by the same amount each year, then Δ would be zero in each of the five years.

Figure 2 shows the year-to-year relative stability of CERES and MODIS radiances as defined in Eq. (2) between 2001 and 2005 for the 0.65- (red) and 0.86- μm (near-infrared) bands. In both bands, CERES and

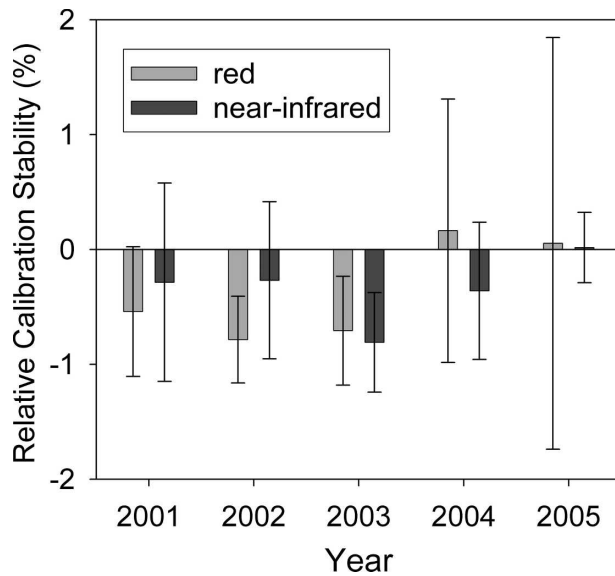


FIG. 2. The year-to-year relative calibration stability of CERES and MODIS determined by comparing predicted mean radiances from regression relations in each year with predicted mean radiances from regression relations derived in 2000 [see Eq. (2)].

MODIS radiances have remained stable relative to one another to better than 1%. Between 2001 and 2003, Δ is negative in both channels, while it is close to 0% for 2004–05. A negative value of Δ can occur if, for a given target, the mean MODIS radiance increases relative to 2000 and CERES radiances remain unchanged. A negative Δ can also occur if the mean CERES radiance decreases relative to 2000 and MODIS radiances remain unchanged. Both of these possibilities imply a decrease in the slopes of regression line fits to data in a given year compared to 2000. Note that from these re-

sults alone, it is not possible to tell which of the above two possibilities has occurred.

Because the CERES measurement is a broadband radiance while the MODIS measurement is a narrowband radiance, a nonzero Δ can also occur if there is a shift in the relative spectral composition of the Tropics with time. For example, any systematic changes in cloud and aerosol properties or their frequency of occurrence (e.g., fewer clouds, lower clouds) will likely have a different effect on the broadband measurement than on the narrowband measurement. If present, such changes could be misinterpreted as relative calibration changes in this analysis.

b. MISR and MODIS Terra radiance comparisons

To assess the relative stability of MISR and MODIS radiances, MISR nadir radiances in the SSFM Edition2B data product (LSMLD) are directly compared with MODIS nadir radiances in the SSF data product. Radiances from both instruments have been averaged over the same CERES footprints and weighted by the CERES PSF. Because MISR and MODIS are narrowband instruments with similar spectral bands, the relative stability of their radiances can be determined with fewer days than what is needed to compare CERES and MODIS. In addition, any changes in the relative spectral composition of the Tropics with time will have a much smaller influence in the MISR/MODIS comparison than the CERES/MODIS comparison. Two September days per year for every year between 2000 and 2004 (10 days total) are used to compare MISR and MODIS. Figures 3a and 3b show scatterplots of MISR and MODIS radiances from 12 September 2000, in the red and near-infrared bands,

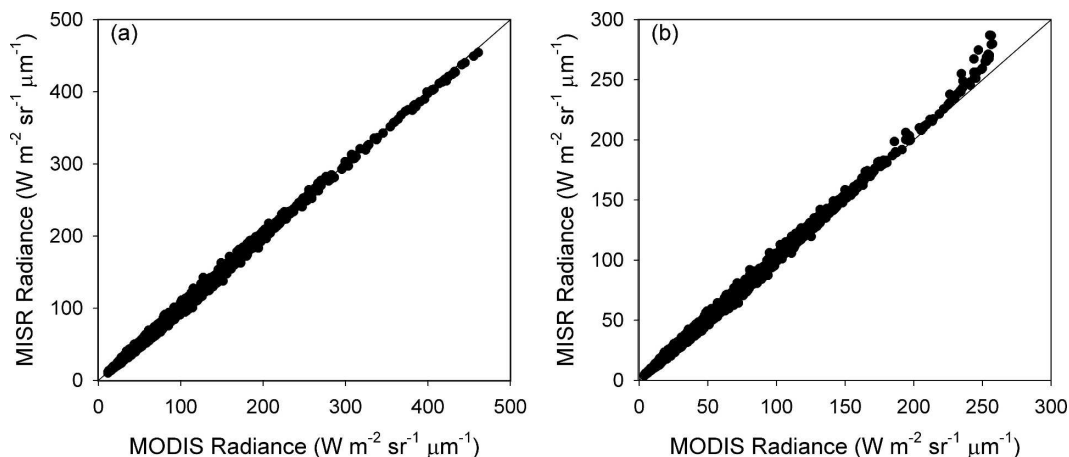


FIG. 3. Scatterplot of footprint average MISR and MODIS (a) red and (b) near-infrared radiances for all CERES footprints over ocean between 30°S and 30°N on 12 Sep 2000. One-to-one line is indicated.

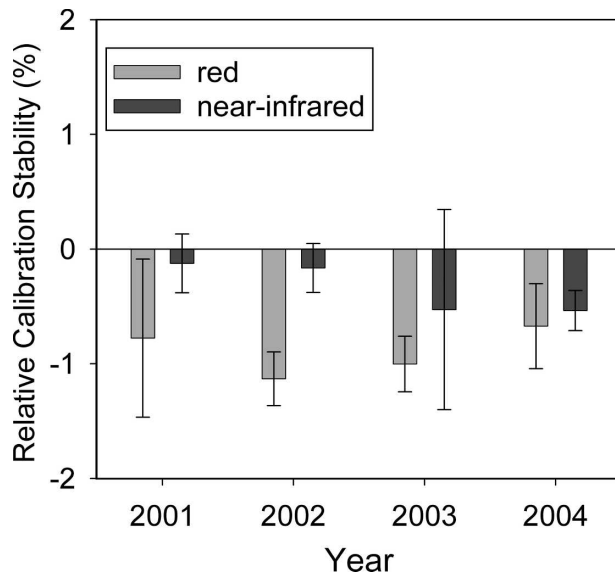


FIG. 4. Same as in Fig. 2, but for MISR and MODIS.

respectively. Each point corresponds to an individual instantaneous footprint average radiance. In the red band (Fig. 3a), the correlation is excellent, with $r^2 = 0.999$ and $CV = 3.2\%$. In the near-infrared band, the MODIS saturates for very bright scenes, as is clearly evident from Fig. 3b. To avoid introducing errors due to saturation, only MODIS near-infrared radiances smaller than $200 \text{ W m}^{-2} \text{ sr}^{-1} \mu\text{m}^{-1}$ are considered. With this criterion, the r^2 for MISR and MODIS near-infrared radiances is 0.998 and CV is 3.6%.

Linear regression fits are derived from MISR and MODIS radiances from each of the 10 available September days between 2000 and 2004. The regression coefficients from each day are then applied to produce 10 sets of predicted red and near-infrared MISR radiances averaged over the tropical oceans [cf. Eq. (1)]. The relative stability of MISR and MODIS radiances is determined by comparing predicted mean MISR radiances in a given year with the predicted radiances in 2000.

Figure 4 shows the year-to-year relative stability of MISR and MODIS radiances as defined in Eq. (2) between 2001 and 2004 for the 0.65- (red) and 0.86- μm (near-infrared) bands. The relative stability of MISR and MODIS radiances is better than 1% in the red band and 0.5% in the near-infrared band. Interestingly, in all comparisons Δ is negative. As noted earlier, Δ was also generally negative for the same period in the CERES and MODIS comparisons (Fig. 2). Thus, it would appear that for the same target either MODIS radiances increase relative to 2000 or both CERES and MISR radiances decrease relative to 2000. Again, from

these data alone, it is only possible to identify relative changes in radiance between the instruments, not the actual radiance change of the individual instruments.

A relative stability of 1% or better between CERES, MODIS, and MISR radiances is encouraging. As noted earlier, Ohring et al. (2005) state that in order to meet climate requirements, imager visible radiances used to infer trends in visible cloud optical depth need to be stable to $1\% (\text{decade})^{-1}$, while Earth Radiation Budget measurements need to be stable to 0.3%. As the differences between CERES, MODIS, and MISR radiances in Figs. 2 and 4 show no systematic temporal dependence, the results are not inconsistent with the requirements in Ohring et al. (2005). Clearly, a longer time series is needed to verify this.

4. Deseasonalized anomalies

To compare climate data records from different instruments, it is convenient to compare anomalies in the monthly time series after removing the seasonal cycle in the data. A deseasonalized monthly anomaly is determined by differencing the average in a given month from the average of all years of the same month. Deseasonalized anomalies of a variable X are determined as follows:

$$\Delta X(\text{yr}, \text{mn}) = X(\text{yr}, \text{mn}) - \bar{X}(\text{mn}), \quad (6)$$

where $X(\text{yr}, \text{mn})$ is the monthly mean of X in year “yr” and month “mn,” and $\bar{X}(\text{mn})$ is the average of X from all years of month mn.

a. CERES Terra SW TOA flux and SeaWiFS PAR

Figure 5a shows deseasonalized monthly anomalies in SeaWiFS PAR and CERES FM1 SW TOA flux over ocean for 30°S – 30°N from March 2000 through June 2005. Since PAR is an estimate of the 400–700-nm radiation reaching the surface and CERES SW flux is an estimate of the reflected solar flux at the TOA, the two are anticorrelated. The CERES SW TOA flux anomalies remain relatively constant throughout the period except for a brief decrease during the second half of 2003, followed by rapid fluctuations in early 2004. The maximum SW TOA flux anomaly in March 2004 coincides with the minimum anomaly in PAR. The March 2004 anomaly is approximately 4 times larger than the standard deviation in monthly anomalies for the entire period.

When SW TOA flux and PAR anomalies are plotted against one another, the r^2 value is 0.93 and the slope of the regression line is $-6.60 \text{ W m}^{-2} \text{ per E m}^{-2} \text{ day}^{-1}$. Figure 5b shows the same results as in Fig. 5a after scaling the PAR monthly anomalies by the slope of the regression line. The correspondence between the

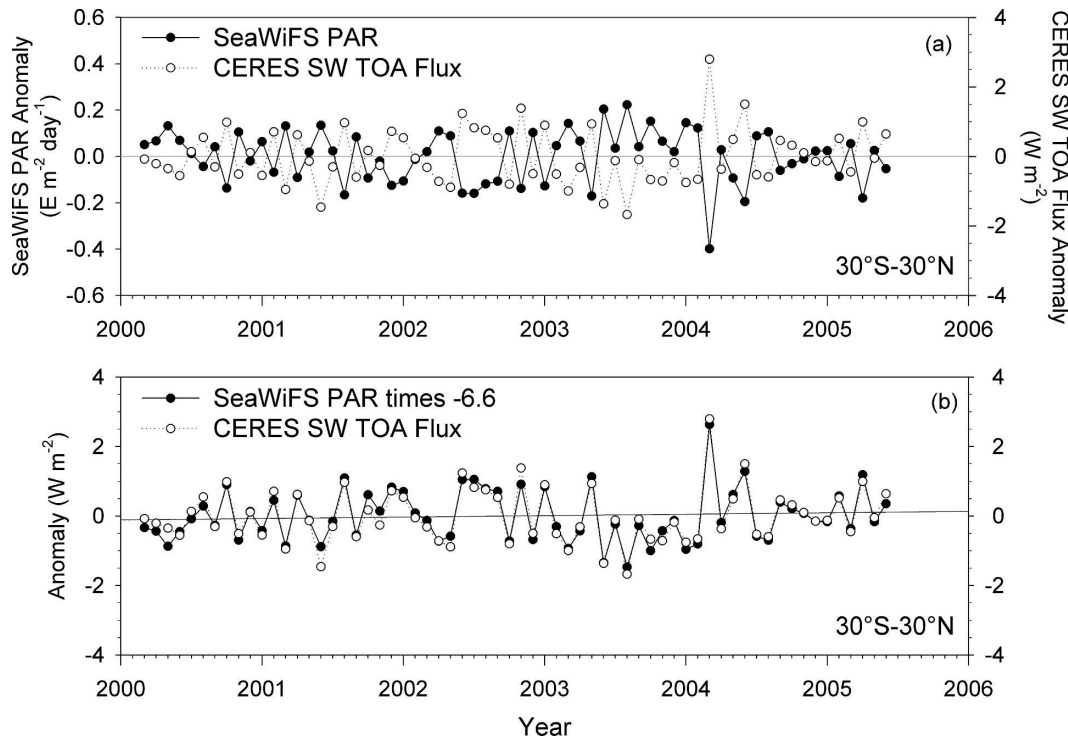


FIG. 5. (a) Deseasonalized monthly anomalies in SeaWiFS PAR ($\text{Einstein m}^{-2} \text{ day}^{-1} = 2.51726 \text{ W m}^{-2}$) and CERES *Terra* FM1 SW TOA flux (W m^{-2}) over ocean for 30°S – 30°N from March 2000 to June 2005; (b) same as in (a), except that SeaWiFS PAR anomalies are scaled by a factor of -6.60 , corresponding to the slope of the regression line fit relating CERES SW TOA flux and SeaWiFS PAR anomalies. The solid and dotted lines without symbols in (b) correspond to regression line fits to the SeaWiFS and CERES anomalies, respectively.

CERES and SeaWiFS anomalies is quite remarkable. The standard deviation in the monthly anomalies for both data records is approximately 0.8 W m^{-2} , and the standard deviation in the difference between CERES and SeaWiFS monthly anomalies is 0.21 W m^{-2} (Table 2), a factor of 4 smaller than the month-to-month variability. Neither CERES *Terra* nor SeaWiFS indicates any significant systematic change during the period considered (Table 3). The slope in the SeaWiFS anomalies is $0.41 \pm 1.2 \text{ W m}^{-2} \text{ decade}^{-1}$, compared to $0.43 \pm 1.5 \text{ W m}^{-2} \text{ decade}^{-1}$ for CERES. The two are consistent to $0.02 \pm 0.3 \text{ W m}^{-2} \text{ decade}^{-1}$, where $\pm 0.3 \text{ W m}^{-2} \text{ decade}^{-1}$ corresponds to the 95% confidence interval. This difference comes very close to falling within the $0.3 \text{ W m}^{-2} \text{ decade}^{-1}$ stability requirement in Ohring et al. (2005). Part of the difference between SeaWiFS and CERES may occur because SeaWiFS PAR is a narrowband (0.4 to $0.7 \mu\text{m}$) quantity while CERES SW TOA flux is broadband.

We note that systematic trends in cloud properties can alter the narrow-to-broadband relationship between CERES and SeaWiFS, and influence the SeaWiFS–CERES anomaly comparison. To illustrate, we have repeated the analysis in Fig. 5 for the four

tropical ocean regions listed in Table 4. In two of the regions considered (southwest and northwest tropical ocean regions), SeaWiFS–CERES anomaly trends are significantly different. These differences are accompanied by significant changes in low cloud cover, as shown in Table 4. In the southwest tropical ocean region, the SeaWiFS–CERES anomaly difference decreases as low cloud fraction increases, and the opposite occurs in the northwest tropical ocean region. The change in cloud cover alters the narrow-to-broadband relationship between SW flux and PAR with time, leading to different anomaly trends. For the entire tropical ocean region, cloud property changes are much smaller and the SeaWiFS–CERES anomaly trends are much more consistent.

Regional narrowband–broadband differences between the SeaWiFS and CERES measurements also influence the slope of the regression line between SW TOA flux and PAR anomalies. While the -6.60 W m^{-2} per $\text{E m}^{-2} \text{ day}^{-1}$ regression line slope obtained in this analysis is consistent with radiative transfer calculations for typical cloud and aerosol conditions (not shown), the slope does show some sensitivity to regional variations in cloud and aerosol properties. Figure 6 shows

TABLE 2. Summary of monthly anomaly statistics for each data record comparison; σ is the standard deviation in monthly anomalies; $\sigma(D)$ is the standard deviation of the difference between monthly anomalies from two data records.

Time period/region	Variable	σ (W m^{-2})	$\sigma(D)$ (W m^{-2})	r^2
Mar 2000–Jun 2005	SeaWiFS PAR	0.76	0.21	0.93
30°S–30°N (ocean)	CERES <i>Terra</i> SW TOA flux	0.79		
Mar 2000–Jun 2005	CERES <i>Terra</i> SW TOA flux	0.83	—	—
30°S–30°N				
Mar 2000–Jun 2005	CERES <i>Terra</i> SW TOA flux	0.32	—	—
30°S–30°N (land)				
Mar 2000–Jun 2005	CERES <i>Terra</i> SW TOA flux	0.55	—	—
90°S–90°N				
Aug 2002–Mar 2005	CERES <i>Aqua</i> SW TOA flux	0.77	0.42	0.75
30°S–30°N	CERES <i>Terra</i> SW TOA flux	0.81		
Aug 2002–Mar 2005	CERES <i>Aqua</i> SW TOA flux	0.44	0.36	0.48
90°S–90°N	CERES <i>Terra</i> SW TOA flux	0.48		
Mar 2000–Dec 2004	ISCCP SW TOA flux	1.2	0.91	0.43
30°S–30°N	CERES <i>Terra</i> SW TOA flux	0.85		
Mar 2000–Dec 2004	ISCCP SW TOA flux	1.1	0.97	0.19
90°S–90°N	CERES <i>Terra</i> SW TOA flux	0.56		

TABLE 3. Summary of monthly anomaly trends and uncertainties.

Time period/region	Variable	Slope ($\text{W m}^{-2} \text{ decade}^{-1}$)	95% confidence interval in slope ($\text{W m}^{-2} \text{ decade}^{-1}$)	Slope of anomaly difference ($\text{W m}^{-2} \text{ decade}^{-1}$)
Mar 2000–Jun 2005	SeaWiFS PAR	0.41	(−0.8, 1.6)	−0.02 ± 0.3
30°S–30°N (ocean)	CERES <i>Terra</i> SW TOA flux	0.43	(−0.9, 2.0)	
Mar 2000–Jun 2005	CERES <i>Terra</i> SW TOA flux	−0.26	(−1.6, 1.1)	—
30°S–30°N				
Mar 2000–Jun 2005	CERES <i>Terra</i> SW TOA flux	−0.69	(−1.2, −0.2)	—
30°S–30°N (land)				
Mar 2000–Jun 2005	CERES <i>Terra</i> SW TOA flux	−0.59	(−1.5, 0.3)	—
90°S–90°N				
Aug 2002–Mar 2005	CERES <i>Aqua</i> SW TOA flux	−3.5	(−6.9, −0.073)	−3.5 ± 1.5
30°S–30°N	CERES <i>Terra</i> SW TOA flux	0.031	(−3.8, 3.9)	
Aug 2002–Mar 2005	CERES <i>Aqua</i> SW TOA flux	−2.9	(−4.7, −1.1)	−3.8 ± 1.0
90°S–90°N	CERES <i>Terra</i> SW TOA flux	0.93	(−1.3, 3.2)	
Mar 2000–Dec 2004	ISCCP SW TOA flux	0.75	(−1.5, 3.0)	1.4 ± 1.7
30°S–30°N	CERES <i>Terra</i> SW TOA flux	−0.64	(−2.3, 1.0)	
Mar 2000–Dec 2004	ISCCP SW TOA flux	1.8	(−0.2, 3.8)	2.5 ± 1.7
90°S–90°N	CERES <i>Terra</i> SW TOA flux	−0.76	(−1.8, 0.3)	

TABLE 4. Slope of SeaWiFS and CERES anomaly difference (SeaWiFS minus CERES) and low cloud fraction anomaly by region. Low cloud fraction anomalies are based on MODIS–SSF retrievals. Low clouds are defined as clouds with effective pressures greater than 680 mb.

Region	Latitude/longitude range	Slope of SeaWiFS–CERES anomaly difference ($\text{W m}^{-2} \text{ decade}^{-1}$)	Slope of low cloud fraction anomaly (decade^{-1})
Southwest tropical ocean	30°S–0° 180°–0°	−2.8 ± 0.95	0.030 ± 0.018
Southeast tropical ocean	30°S–0° 0°–180°	−0.058 ± 1.0	−0.013 ± 0.018
Northwest tropical ocean	0°–30°N 180°–0°W	2.1 ± 0.89	−0.031 ± 0.024
Northeast tropical ocean	0°–30°N 0°–180°	0.72 ± 0.84	0.0004 ± 0.0067
Tropical ocean	30°S–30°N 180°	−0.02 ± 0.3	0.0023 ± 0.0088

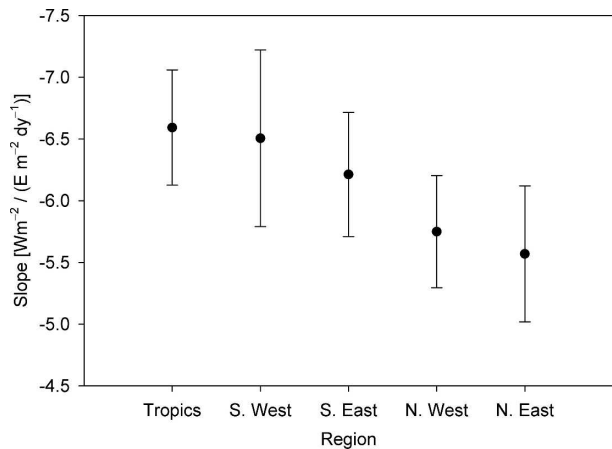


FIG. 6. Slope of the SeaWiFS PAR-CERES SW flux anomaly regression line for the tropical ocean regions listed in Table 4.

the slope of the SeaWiFS PAR-CERES SW flux anomaly regression line for the tropical ocean regions listed in Table 4. For these relatively large-scale oceanic regions, the slope varies by approximately 15%. Larger differences are expected over land and snow.

Interestingly, the slope in the CERES *Terra* SW

TOA flux anomalies for the entire Tropics (ocean and land) is of the opposite sign to that for ocean only (Table 3). For the entire Tropics, the slope is $-0.26 \pm 1.3 \text{ W m}^{-2} \text{ decade}^{-1}$ compared to $0.43 \pm 1.5 \text{ W m}^{-2} \text{ decade}^{-1}$ for ocean only. This difference is associated with SW TOA flux changes over land. Figure 7a shows the land SW TOA flux anomalies averaged over the Tropics together with the multivariate ENSO index (MEI; Wolter and Timlin 1993, 1998). The land SW TOA flux anomalies decrease by $-0.69 \pm 0.5 \text{ W m}^{-2} \text{ decade}^{-1}$ and are anticorrelated with the MEI, as indicated in Fig. 7b (the slope of the line in Fig. 7b is $-0.33 \pm 0.14 \text{ W m}^{-2}$). These results suggest that SW TOA fluxes tend to be smaller over land during El Niño events and larger during periods of La Niña. In contrast, a similar scatterplot of tropical ocean SW TOA flux anomalies versus MEI failed to show a significant relationship (not shown). For the entire globe, the decrease in reflectance is more pronounced, at $-0.59 \pm 0.9 \text{ W m}^{-2} \text{ decade}^{-1}$.

b. CERES *Terra* and CERES *Aqua* SW TOA Flux

A direct comparison of SW TOA flux anomalies from CERES *Terra* FM1 and CERES *Aqua* FM4 for

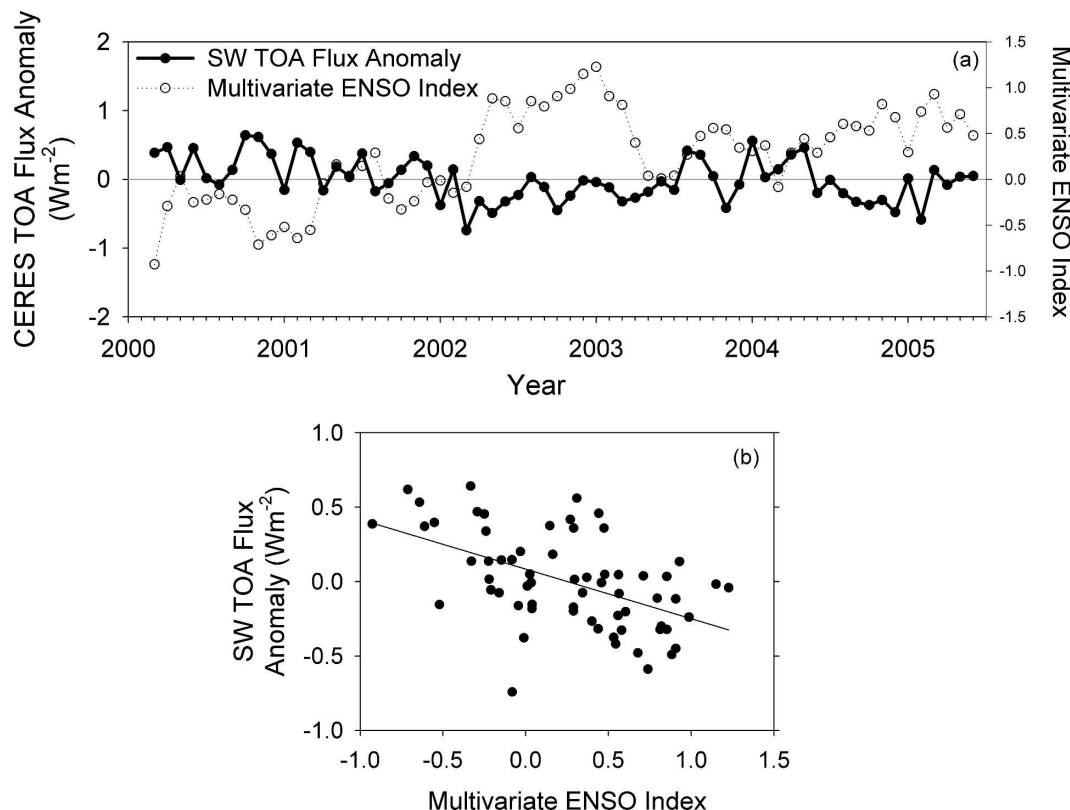


FIG. 7. (a) Deseasonalized monthly anomaly in CERES SW TOA flux for land and multivariate ENSO index for 30°S – 30°N ; (b) scatterplot of CERES monthly SW TOA flux anomaly and multivariate ENSO index.

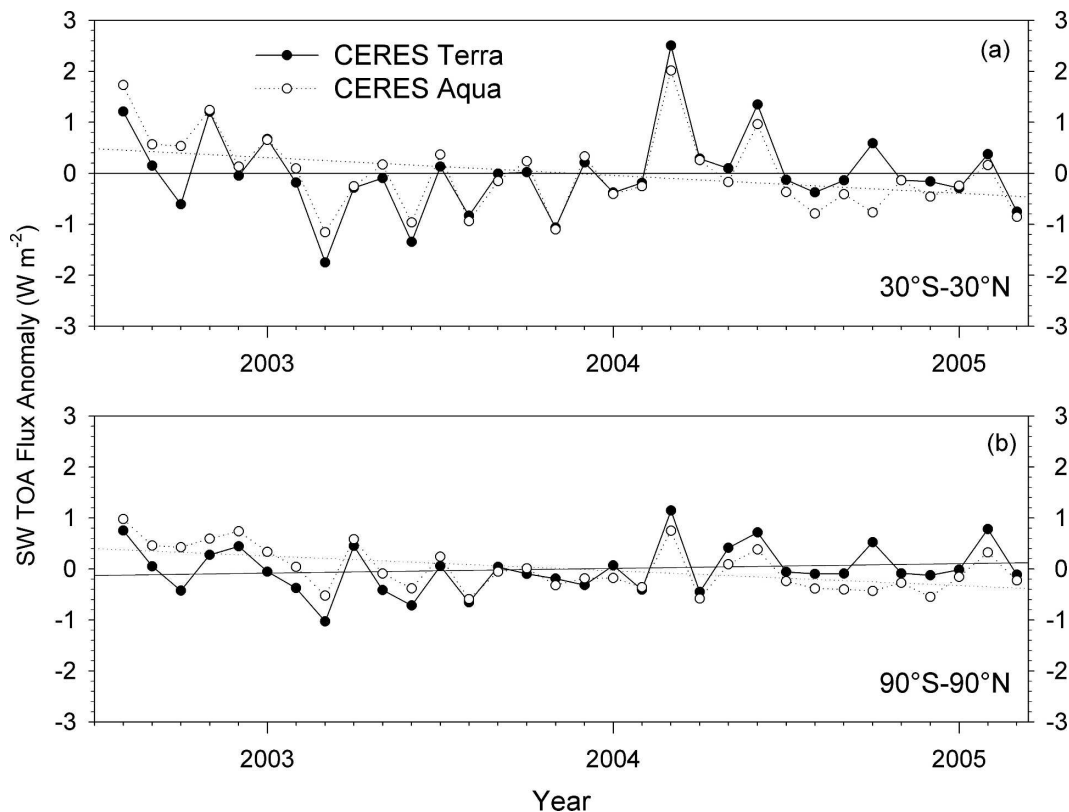


FIG. 8. (a) Deseasonalized monthly anomalies in CERES *Terra* FM1 and CERES *Aqua* FM4 all-sky SW TOA flux (W m^{-2}) for (a) 30°S – 30°N and (b) 90°S – 90°N from August 2002 to March 2005. The solid and dotted lines without symbols correspond to regression line fits to the anomalies.

August 2002 through March 2005 is provided in Figs. 8a and 8b. During the first 12 months (up to July 2003), CERES *Aqua* SW TOA flux anomalies exceed those of CERES *Terra*, while the opposite is true during the last 13 months from March 2004 through March 2005. The CERES *Aqua* TOA fluxes systematically decrease by $3.5 \text{ W m}^{-2} \text{ decade}^{-1}$ in the Tropics and $2.9 \text{ W m}^{-2} \text{ decade}^{-1}$ for the globe (Table 3), while CERES *Terra* anomalies remain relatively constant [$<1 \text{ W m}^{-2} \text{ decade}^{-1}$]. Both records indicate that the variability in all-sky SW TOA fluxes in the Tropics exceeds that for the entire globe by approximately 70% (Table 2). While the standard deviation in the CERES *Aqua* and *Terra* monthly anomalies is consistent to 0.4 W m^{-2} , the correlation between the two records is quite low— r^2 is only 0.75 for the Tropics and 0.47 for the globe.

As is indicated in Table 3, the difference between the slope of the regression lines in Figs. 8a and 8b is significant at the 95% level. The discrepancy is believed to be due to uncertainties in the adjustment factors used to account for degradation of the CERES FM4 SW channel optics during hemispheric scan mode operations. While such adjustments are made for both

CERES FM1 and FM4, the methodology used to derive the adjustment factors was found to work far better for CERES *Terra* than for CERES *Aqua*, suggesting that either FM4 optics continued to degrade in cross-track mode or the FM4 onboard lamb got brighter during the mission (as was observed with the CERES instrument on the Tropical Rainfall Measuring Mission satellite).

c. CERES *Terra* and ISCCP FD RadFlux SW TOA Flux

Figures 9a and 9b compare SW TOA flux anomalies from CERES *Terra* and the ISCCP FD RadFlux data product (Zhang et al. 2004) for March 2000 through December 2004. ISCCP FD RadFlux anomalies show approximately 40% more variability than CERES *Terra* in the Tropics, and are almost twice as variable as CERES *Terra* globally (Table 2). The correlation between the two data records is also quite low, with r^2 values of 0.43 in the Tropics and 0.19 globally. Interestingly, the month-to-month agreement between the two data records is markedly better from January 2002 onward compared to the first 22 months. ISCCP radia-

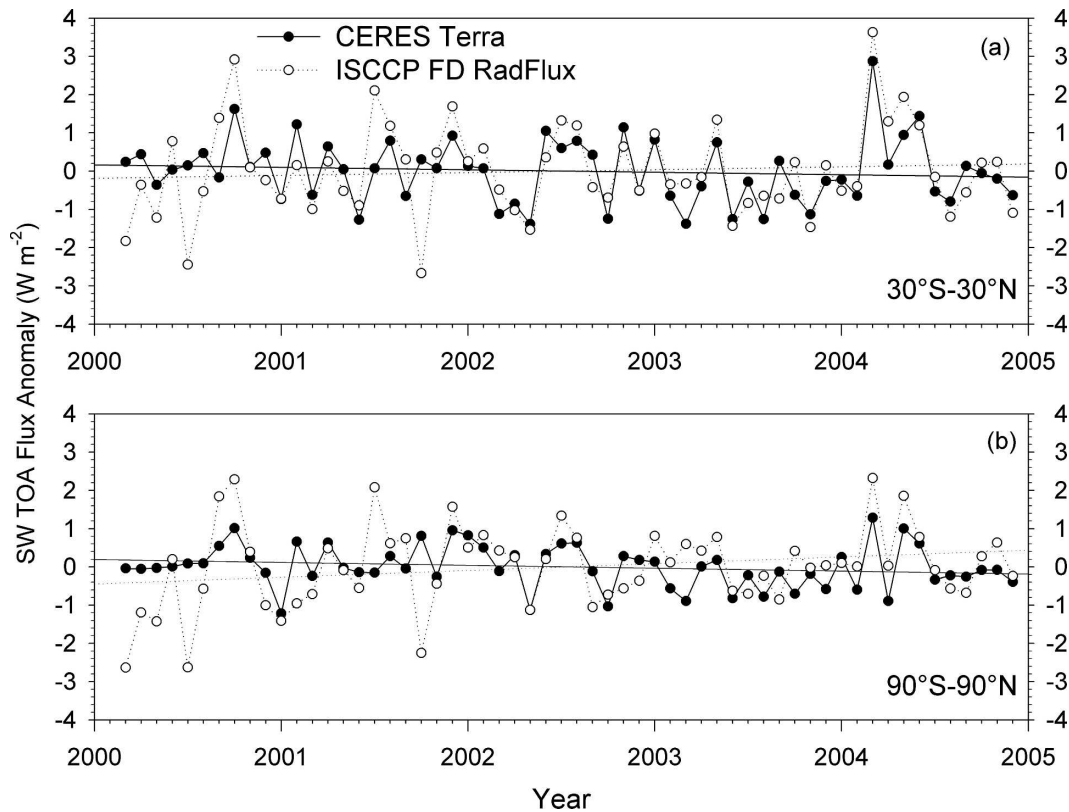


FIG. 9. (a) Deseasonalized monthly anomalies in CERES *Terra* FM1 and ISCCP FD RadFlux all-sky SW TOA flux (W m^{-2}) for (a) 30°S – 30°N and (b) 90°S – 90°N from August 2002 to March 2005. The solid and dotted lines without symbols correspond to regression line fits to the anomalies.

tive flux anomalies prior to January 2002 are far more variable than both CERES *Terra* anomalies and ISCCP anomalies after January 2002.

In the Tropics, both ISCCP and CERES *Terra* SW TOA flux anomalies show modest changes (Table 3). ISCCP anomalies increase by $0.75 \pm 2.3 \text{ W m}^{-2} \text{ decade}^{-1}$ while CERES *Terra* anomalies decrease by $0.64 \pm 1.5 \text{ W m}^{-2} \text{ decade}^{-1}$. Globally, the ISCCP SW TOA flux anomalies show a much larger increase of $1.8 \pm 2 \text{ W m}^{-2} \text{ decade}^{-1}$, while CERES *Terra* anomalies decrease by $0.76 \pm 1 \text{ W m}^{-2} \text{ decade}^{-1}$. While neither of these changes is significant at the 95% level, the difference in the slopes is significant ($2.5 \pm 1.7 \text{ W m}^{-2} \text{ decade}^{-1}$). We note that despite these differences, the ISCCP results fall well within the 3%–5% relative calibration uncertainty estimated by Brest et al. (1997).

d. Trend analysis

The recent advances in technology and onboard calibration have led to significant improvements in the radiometric stability of current state-of-the-art satellite

instruments such as those considered in this study. Older instruments such as the Advanced Very High Resolution (AVHRR) series of sensors, which had no onboard calibration in the visible channels typically degraded by 1%–3% per year (Brest et al. 1997; Tahnk and Coakley 2001). If the newer instruments continue to collect data until the spacecraft they fly on exhaust all of the available fuel (nominally 15 yr for *Terra* and *Aqua*), how small a trend can we expect to be able to observe, assuming instrument calibration remains stable? The question is critical given that greenhouse gas radiative forcing is approximately $0.6 \text{ W m}^{-2} \text{ decade}^{-1}$ (Houghton et al. 2001), and a 50% change in climate sensitivity due to cloud feedback would arise from a net cloud radiative effect change of only $0.3 \text{ W m}^{-2} \text{ decade}^{-1}$: either stabilizing or destabilizing. Narrowing climate prediction uncertainty to a factor of 2 thus requires verification of cloud feedback at the level of 0.3 W m^{-2} change per decade. According to Weatherhead et al. (1998), trend detectability depends upon three major factors: (i) the size of the trend to be detected; (ii) the unexplained variability in the data (e.g., natural climate variability); and (iii) the autocorrelation

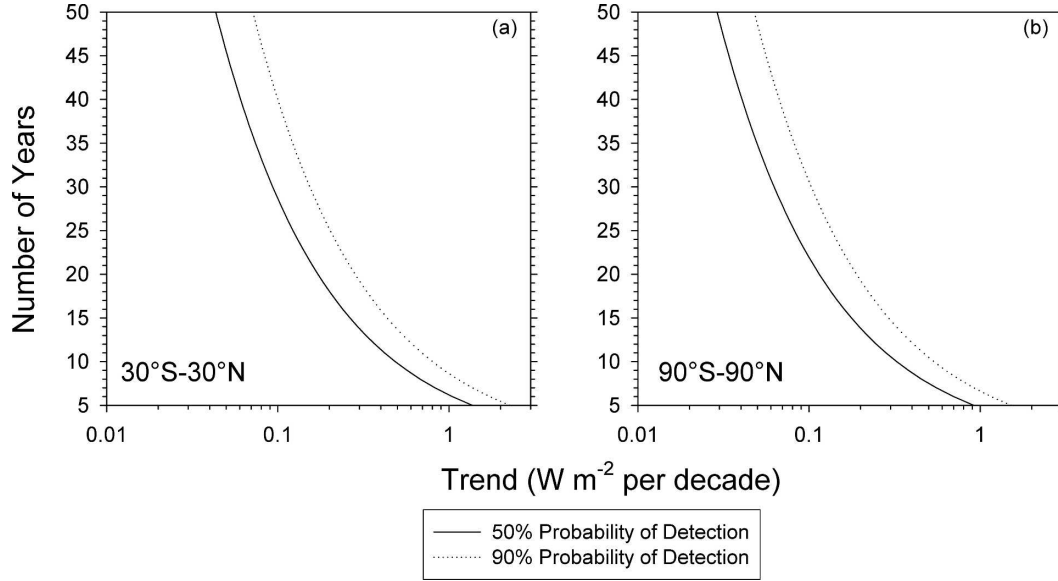


FIG. 10. Number of years to detect a given trend in SW TOA flux anomaly with 50% and 90% probability for (a) 30°S–30°N and (b) 90°S–90°N.

of the noise in the data. Following techniques commonly used to assess trends in environmental data, Weatherhead et al. (2000) derive the following expression to determine the number of years (n^*) required to detect a trend of magnitude ω_o , with at least $1-\beta$ probability:

$$n^* \approx \left[\frac{(2 + z_\beta)}{|\omega_o|} \sigma_N \sqrt{\frac{1 + \phi}{1 - \phi}} \right]^{2/3}, \quad (7)$$

where σ_N is the month-to-month variability in the data, ϕ is the autocorrelation in the month-to-month data with a lag of 1 month, and $-z_\beta$ is the lower β -percentile of the standard normal distribution, such that $P(Z < -z_\beta) = \beta$. Here Z is the standard normal random variate of the estimated trend. From Weatherhead et al. (2000), setting $z_\beta = 0$ in Eq. (7) provides the number of years needed to detect a trend of magnitude ω_o at the 95% significance level with a probability of 50%. Similarly, using $z_\beta = 1.3$ in Eq. (7) provides the number of years needed to detect a trend of magnitude ω_o at the 95% significance level with a probability of 90%.

Figures 10a and 10b show the number of years needed to detect trends in all-sky tropical and global CERES *Terra* SW TOA flux, respectively, with probabilities of 50% and 90%. We assume that the CERES *Terra* instrument calibration remains stable throughout the record and ignore any unforeseen events (e.g., major volcanic eruptions) that may significantly alter the variability and autocorrelation in the data collected af-

ter the initial first 5 yr. To detect a trend in global SW TOA flux that is 50% of the 0.6 W m^{-2} anticipated change in anthropogenic radiative forcing over the next few decades, approximately 10 to 15 yr of data are needed (the lower bound occurs with 50% probability, while the upper bound occurs with 90% probability). Because the variability is greater in the Tropics, the number of years to detect a $0.3 \text{ W m}^{-2} \text{ decade}^{-1}$ trend is also greater, at 14 to 20 yr.

5. Discussion

The results presented in this study are in stark contrast to those of Pallé et al. (2004, 2005), who claim to have observed a 6 W m^{-2} increase in annual mean reflected solar radiation between 2000 and 2003 based on Earthshine measurements. As noted by Wielicki et al. (2005), an increase of 6 W m^{-2} is a factor 2.4 times larger than the anomaly caused by the Mount Pinatubo eruption. Since there is no evidence of a significant event (such as a volcanic eruption) between 2000 and 2003 large enough to produce such a dramatic change in the earth's reflectance, it is unclear why the Earthshine anomaly is so large. When the global monthly anomalies in CERES *Terra* SW TOA flux in Fig. 9b are averaged annually, the difference between the minimum and maximum yearly anomalies is 0.6 W m^{-2} , an order of magnitude smaller than the change found in the Earthshine data. Given the remarkable consistency shown here between data records from CERES, MODIS,

MISR, SeaWiFS, and ISCCP, none of these additional data records support a 6 W m^{-2} change between 2000 and 2003.

Trends of even a few tenths of a percent in global reflected SW flux can have a significant effect on climate sensitivity if uncompensated for by greenhouse cloud effects (e.g., low cloud changes). For example, if the anthropogenic forcing of climate is $0.6 \text{ W m}^{-2} \text{ decade}^{-1}$ (Houghton et al. 2001), a trend of $-0.6 \text{ W m}^{-2} \text{ decade}^{-1}$ in global reflected SW flux would be sufficient to double global temperature climate sensitivity; a trend of $+0.3 \text{ W m}^{-2} \text{ decade}^{-1}$ would reduce climate sensitivity in half. Clearly, some of the SW flux trends due to clouds will likely be compensated by greenhouse thermal infrared effects of clouds. The magnitude of the compensation will depend upon whether the changes occur in low or high clouds: if the changes are dominated by low cloud changes, then compensation by greenhouse thermal infrared effects of clouds will be small; conversely, if the changes occur in high clouds, significantly stronger compensation is likely.

6. Summary and conclusions

Data from several state-of-the-art satellite instruments currently in orbit were analyzed and compared in order to determine if data records emerging from these instruments are meeting climate accuracy goals established by the climate community (Ohring et al. 2005). The relative stability of radiance measurements from CERES, MODIS, and MISR aboard the *Terra* spacecraft during the first 5 yr of operation is determined from a regression analysis of highly collocated and coincident nadir radiances from the three instruments. To determine the relative stability of CERES and MODIS radiances, CERES FM1 cross-track SW radiances and MODIS radiances in the 0.65- (band 1) and 0.86- μm (band 2) bands from the CERES SSF product are used. Each day, average tropical ocean CERES SW and MODIS narrowband radiances are calculated from 1° latitude–longitude equal-area average values. A linear regression fit is applied to the daily tropical averages for each month CERES FM1 operates in cross-track mode during the 5-yr period. The regression equations in each month and year are used to produce a time series of predicted monthly tropical mean CERES SW radiances from the MODIS radiances in each band. The year-to-year relative stability of CERES and MODIS radiances is determined by comparing predicted mean CERES radiances from regression coefficients in each month and year with the predicted mean radiance in the year 2000 for the corresponding month.

In both bands, CERES and MODIS radiances have remained stable relative to one another to better than 1%. Between 2001 and 2003, either MODIS radiances increased slightly relative to 2000 or CERES radiances decreased slightly.

To compare MODIS and MISR nadir radiances, a new merged CERES and MISR dataset (called the SSFM data product) that spatially averages MISR radiances over CERES footprints in the same manner as MODIS radiances are averaged on the CERES SSF product is used. Coincident MISR and MODIS data from 10 September days between 2000 and 2004 are considered. For each day, a regression line is fit to instantaneous MISR and MODIS data over the tropical oceans. The relative stability of MISR and MODIS radiances is determined by comparing predicted mean MISR radiances in a given year with the predicted radiances in 2000. We find that the MISR and MODIS radiances have remained stable relative to one another to better than 1% in the red band and 0.5% in the near-infrared band. Also, the relative changes in MISR and MODIS radiances with time are quite similar to those for CERES and MODIS during the same period. Between 2001 and 2004, either MODIS radiances increased relative to 2000, or both CERES and MISR radiances decreased relative to 2000. From these data alone, it is only possible to identify relative radiance changes between the instruments, not the actual radiance change of the individual instruments. Nevertheless, the results are encouraging. The relative stability of CERES, MODIS, and MISR radiances shows no obvious systematic temporal dependence. Therefore, if the instruments continue to maintain their current levels of stability throughout the mission, results in this study suggest that climate data records from these instruments are likely to meet the climate accuracy goals outlined in Ohring et al. (2005).

One of the most stable earth-viewing satellite instruments in orbit is the SeaWiFS instrument, whose radiances have been shown to be stable to better than 0.07% during the six years in orbit. When deseasonalized anomalies in tropical ocean mean CERES SW TOA flux are compared with SeaWiFS PAR retrievals, the two are strongly anticorrelated. After scaling the SeaWiFS PAR anomalies by the slope of a regression line fit between CERES SW TOA flux and SeaWiFS PAR anomalies in order to place the two data records on the same radiometric scale, the monthly anomalies from the two datasets are consistent to 0.2 W m^{-2} , and the difference between their linear trends is $0.02 \pm 0.3 \text{ W m}^{-2} \text{ decade}^{-1}$ (with 95% confidence). The agreement is close to the $0.3 \text{ W m}^{-2} \text{ decade}^{-1}$ stability re-

quirement outlined in Ohring et al. (2005). In contrast to recent Earthshine results of Pallé et al. (2004, 2005), neither CERES *Terra* nor SeaWiFS indicates any significant systematic change in SW radiative flux during the period considered.

Despite the excellent agreement between CERES and SeaWiFS anomaly trends over the entire Tropics, significant differences were observed when anomalies over smaller areas, such as the southwest and northwest Tropics, were compared. The most likely reason for the different regional trends is changes in cloud and aerosol properties. Such changes can alter the narrow-to-broadband relationship between SW flux and PAR with time, leading to different anomaly trends. Therefore, in order to obtain an accurate quantitative account of long-term changes in both regional and global TOA radiation, stable measurements of the entire SW spectral region are necessary.

While the tropical ocean mean CERES *Terra* and SeaWiFS data records show excellent agreement, the same is not true of CERES *Terra* and CERES *Aqua*. For the period of August 2002 through March 2005, CERES *Aqua* TOA fluxes systematically decrease by $3.5 \text{ W m}^{-2} \text{ decade}^{-1}$ in the Tropics and $2.9 \text{ W m}^{-2} \text{ decade}^{-1}$ for the globe, while CERES *Terra* anomalies remain smaller than $1 \text{ W m}^{-2} \text{ decade}^{-1}$. The difference between the slopes of the regression lines is significant at the 95% level. This discrepancy is believed to be due to the adjustment factors used to account for ultraviolet radiation exposure of the CERES *Aqua* optics during hemispheric scan mode operations. Efforts are underway to improve these corrections.

The CERES *Terra* SW TOA flux anomalies were also compared with those from the ISCCP FD RadFlux data product for March 2000 through December 2004. In general, the correlation between the two data records is also quite low, with r^2 values of 0.43 in the Tropics and 0.19 globally. Global trend differences between these records as determined from the difference between the slopes of regression line fits to the two data records are significant ($2.5 \pm 1.7 \text{ W m}^{-2} \text{ decade}^{-1}$). We note that most of the discrepancy is mainly due to differences in monthly anomalies between March 2000 and January 2002. During this period, ISCCP radiative flux anomalies are highly variable compared to those of CERES *Terra* for the same period and ISCCP anomalies after January 2002.

Given that greenhouse gas radiative forcing is approximately $0.6 \text{ W m}^{-2} \text{ decade}^{-1}$ (Houghton et al. 2001), and a 50% change in climate sensitivity due to cloud feedback would arise from a net cloud radiative effect change of only $0.3 \text{ W m}^{-2} \text{ decade}^{-1}$, the question

arises as to how long a data record would be needed to detect a trend of this magnitude in observations of global SW TOA flux, given the natural variability and autocorrelation in the data. Common statistical techniques were used to address this question under the assumption that CERES *Terra* calibration remains highly stable and long-term climate variability remains constant during the *Terra* record. Results show that in order to detect a $0.3 \text{ W m}^{-2} \text{ decade}^{-1}$ trend in global SW TOA flux, approximately 10 to 15 yr of data are needed.

To take full advantage of the complementary CERES and MODIS data on *Terra* and *Aqua*, a natural follow-on to the present study is to extend the time series analysis to include cloud and aerosol parameters in addition to TOA SW and LW TOA radiative fluxes. The CERES data products facilitate such an analysis because the algorithms and ancillary data used to produce the CERES data products in each "Edition" are kept constant over the entire data record. Such a "frozen" analysis greatly reduces the chances of discovering apparent trends or spurious jumps in the data record that are due to algorithm or input data changes rather than real changes.

Acknowledgments. This work was supported by NASA Clouds and the Earth's Radiant Energy System Grant NNL04AA26G and NASA Grant NNG04GM13G. The research of R. Davies was conducted at the Jet Propulsion Laboratory, California Institute of Technology, under contract with NASA. The CERES SSF and MISR L1B2 data were obtained from the NASA Langley Research Center Atmospheric Sciences Data Center. The ISCCP-FD data were provided by Y.-C. Zhang. The authors thank E. C. Weatherhead for helpful comments regarding the statistical analysis of the data.

REFERENCES

- Barnes, R. A., R. E. Eplee Jr., F. S. Patt, H. H. Kieffer, T. C. Stone, G. Meister, J. J. Butler, and C. R. McClain, 2004: Comparison of SeaWiFS measurements of the moon with the U.S. Geological Survey lunar model. *Appl. Opt.*, **43**, 5838–5854.
- Barnes, W. L., T. S. Pagano, and V. V. Salomonson, 1998: Pre-launch characteristics of the Moderate Resolution Imaging Spectroradiometer (MODIS) on EOS-AM1. *IEEE Trans. Geosci. Remote Sens.*, **36**, 1088–1100.
- , X. Xiaoxiong, and V. V. Salomonson, 2004: MODIS instrument status and operational activities. *Proc. SPIE*, **5542**, doi:10.1117/12.558185.
- Brest, C. L., W. B. Rossow, and M. D. Roiter, 1997: Update of radiance calibrations for ISCCP. *J. Atmos. Oceanic Technol.*, **14**, 1091–1109.

- Bruegge, C. J., N. L. Chrien, R. R. Ando, D. J. Diner, W. A. Abdou, M. C. Helmlinger, S. H. Pilorz, and K. J. Thome, 2002: Early validation of the Multi-angle Imaging SpectroRadiometer (MISR) radiometric scale. *IEEE Trans. Geosci. Remote Sens.*, **40**, 1477–1492.
- Diner, D. J., and Coauthors, 1998: Multiangle Imaging SpectroRadiometer (MISR) description and experiment overview. *IEEE Trans. Geosci. Remote Sens.*, **36**, 1072–1087.
- , J. C. Beckert, G. W. Bothwell, and J. I. Rodriguez, 2002: Performance of the MISR instrument during its first 20 months in Earth orbit. *IEEE Trans. Geosci. Remote Sens.*, **40**, 1449–1466.
- Eplee, R. E., Jr., R. A. Barnes, F. S. Patta, G. Meisterb, and C. R. McClain, 2004: SeaWiFS lunar calibration methodology after six years on orbit. *Proc. SPIE*, **5542**, doi:10.1117/12.556408.
- Geier, E. B., R. N. Green, D. P. Kratz, P. Minnis, W. F. Miller, S. K. Nolan, and C. B. Franklin, cited 2003: Single satellite footprint TOA/surface fluxes and clouds (SSF) collection document. [Available online at http://asd-www.larc.nasa.gov/ceres/collect_guide/SSF_CG.pdf.]
- Hooker, S. B., W. E. Esaias, G. C. Feldman, W. W. Gregg, and C. R. McClain, 1992: An overview of SeaWiFS and ocean color. SeaWiFS Tech. Rep. Series, Vol. 1, NASA Tech. Memo. 104566, 785 pp.
- Houghton, J. T., Y. Ding, D. J. Griggs, M. Noguer, P. J. van der Linden, X. Dai, K. Maskell, and C. A. Johnson, Eds., 2001: *Climate Change 2001: The Scientific Basis*. Cambridge University Press, 881 pp.
- Ignatov, A., and L. L. Stowe, 2002: Aerosol retrievals from individual AVHRR channels. Part I: Retrieval algorithm and transition from Dave to 6S radiative transfer model. *J. Atmos. Sci.*, **59**, 313–334.
- Loeb, N. G., N. M. Smith, S. Kato, W. F. Miller, S. K. Gupta, P. Minnis, and B. A. Wielicki, 2003: Angular distribution models for top-of-atmosphere radiative flux estimation from the Clouds and the Earth's Radiant Energy System instrument on the Tropical Rainfall Measuring Mission Satellite. Part I: Methodology. *J. Appl. Meteor.*, **42**, 240–265.
- , S. Kato, K. Loukachine, and N. M. Smith, 2005: Angular distribution models for top-of-atmosphere radiative flux estimation from the Clouds and the Earth's Radiant Energy System instrument on the Terra satellite. Part I: Methodology. *J. Oceanic Atmos. Technol.*, **22**, 338–351.
- , W. Sun, W. F. Miller, K. Loukachine, and R. Davies, 2006: Fusion of CERES, MISR and MODIS measurements for top-of-atmosphere radiative flux validation. *J. Geophys. Res.*, **111**, D18209, doi:10.1029/2006JD007146.
- Matthews, G., K. J. Priestley, P. Spence, D. Cooper, and D. Walikainen, 2005: Compensation for spectral darkening of short wave optics occurring on the Cloud's and the Earth's Radiant Energy System. *Proc. SPIE*, **5882**, doi:10.1117/12.618972.
- Minnis, P., D. P. Garber, D. F. Young, R. F. Arduini, and Y. Tokano, 1998: Parameterizations of reflectance and effective emittance for satellite remote sensing of cloud properties. *J. Atmos. Sci.*, **55**, 3313–3339.
- , D. F. Young, S. Sun-Mack, P. W. Heck, D. R. Doelling, and Q. Trepte, 2003: CERES Cloud Property Retrievals from Imagers on TRMM, Terra, and Aqua. *Proc. SPIE 10th Int. Symp. on Remote Sensing: Conf. on Remote Sensing of Clouds and the Atmosphere VII*, Barcelona, Spain, SPIE, 37–48.
- Ohring, G., B. A. Wielicki, R. Spencer, B. Emery, and R. Datla, 2005: Satellite instrument calibration for measuring global climate change: Report of a workshop. *Bull. Amer. Meteor. Soc.*, **86**, 1303–1313.
- Pallé, E., P. R. Goode, P. Montañés-Rodríguez, and S. E. Koonin, 2004: Changes in the Earth's reflectance over the past two decades. *Science*, **304**, doi:10.1126/science.1094070.
- , P. Montañés-Rodríguez, P. R. Goode, S. E. Koonin, M. Wild, and S. Casadio, 2005: A multi-data comparison of shortwave climate forcing changes. *Geophys. Res. Lett.*, **32**, L21702, doi:10.1029/2005GL023847.
- Patt, F. S., and Coauthors, 2003: Algorithm updates for the fourth SeaWiFS data reprocessing. S. B. Hooker and E. R. Firestone, Eds., NASA Tech. Memo. 2003–206892, Vol. 22, NASA Goddard Space Flight Center, Greenbelt, MD, 74 pp. [Available online at http://oceancolor.gsfc.nasa.gov/cgi/postlaunch_tech_memo.pl?22.]
- Remer, L. A., and Coauthors, 2005: The MODIS aerosol algorithm, products, and validation. *J. Atmos. Sci.*, **62**, 947–973.
- Rosow, W. B., and R. A. Schiffer, 1999: Advances in understanding clouds from ISCCP. *Bull. Amer. Meteor. Soc.*, **80**, 2261–2287.
- Salomonson, V. V., W. L. Barnes, P. W. Maymon, H. E. Montgomery, and H. Ostrow, 1989: MODIS: Advanced facility instrument for studies of the earth as a system. *IEEE Trans. Geosci. Remote Sens.*, **27**, 145–153.
- Smith, G. L., 1994: Effects of time response on the point spread function of a scanning radiometer. *Appl. Opt.*, **33**, 7031–7037.
- Spence, P., K. J. Priestley, E. Kizer, S. Thomas, D. Cooper, and D. Walikainen, 2004: Correction of drifts in the measurements of the clouds and the earth's radiant energy system scanning thermistor bolometer instruments on the Terra and Aqua satellites. *Proc. SPIE*, **5542**, 53–64.
- Suarez, M. J., 2005: Documentation and validation of the Goddard Earth Observing System (GEOS) data assimilation system—Version 4. Vol. 26, Tech. Rep. Series on Global Modeling and Data Assimilation, NASA/TM-2005-104606, 181 pp.
- Tahnk, W. R., and J. A. Coakley Jr., 2001: Improved calibration coefficients for NOAA-14 AVHRR visible and near-infrared channels. *Int. J. Remote. Sens.*, **22**, 1269–1283.
- Weatherhead, E. C., and Coauthors, 1998: Factors affecting the detection of trends: Statistical considerations and applications to environmental data. *J. Geophys. Res.*, **103**, 17 149–17 161.
- , and Coauthors, 2000: Detecting the recovery of total column ozone. *J. Geophys. Res.*, **105**, 22 201–22 210.
- Wielicki, B. A., B. R. Barkstrom, E. F. Harrison, R. B. Lee III, G. L. Smith, and J. E. Cooper, 1996: Clouds and the Earth's Radiant Energy System (CERES): An Earth observing system experiment. *Bull. Amer. Meteor. Soc.*, **77**, 853–868.
- , and Coauthors, 2002: Evidence for large decadal variability in the tropical mean radiative energy budget. *Science*, **295**, 841–844.
- , T. Wong, N. Loeb, P. Minnis, K. Priestley, and R. Kandel, 2005: Changes in Earth's albedo measured by satellite. *Science*, **308**, 825.
- Wolter, K., and M. S. Timlin, 1993: Monitoring ENSO in COADS with a seasonally adjusted principal component index. *Proc.*

- 17th Climate Diagnostics Workshop*, Norman, OK, NOAA/NMC/CAC, NSSL, Oklahoma Climate Survey, CIMMS, and the School of Meteorology, University of Oklahoma, 52–57.
- , and —, 1998: Measuring the strength of ENSO—How does 1997/98 rank? *Weather*, **53**, 315–324.
- Wong, T., B. A. Wielicki, R. B. Lee III, G. L. Smith, and K. A. Bush, 2006: Reexamination of the observed decadal variability of the earth radiation budget using altitude-corrected ERBE/ERBS Nonscanner WFOV data. *J. Climate*, **19**, 4028–4040.
- Zhang, Y.-C., W. B. Rossow, and A. A. Lacis, 1995: Calculation of surface and top of atmosphere radiative fluxes from physical quantities based on ISCCP data sets: 1. Method and sensitivity to input data uncertainties. *J. Geophys. Res.*, **100**, 1149–1165.
- , —, —, V. Oinas, and M. I. Mishchenko, 2004: Calculation of radiative fluxes from the surface to top of atmosphere based on ISCCP and other global data sets: Refinements of the radiative transfer model and the input data. *J. Geophys. Res.*, **109**, D19105, doi:10.1029/2003JD004457.